Superscattering of Light from Subwavelength Nanostructures

Zhichao Ruan and Shanhui Fan

Ginzton Laboratory, Department of Electrical Engineering, Stanford University, Stanford, California 94305

(Received 9 March 2010; revised manuscript received 2 June 2010; published 28 June 2010)

We provide a theoretical discussion of the scattering cross section of individual subwavelength structures. We show that, in principle, an arbitrarily large total cross section can be achieved, provided that one maximizes contributions from a sufficiently large number of channels. As a numerical demonstration, we present a subwavelength nanorod with a plasmonic-dielectric-plasmonic layer structure, where the scattering cross section far exceeds the single-channel limit, even in the presence of loss.

DOI: 10.1103/PhysRevLett.105.013901 PACS numbers: 42.25.−p, 78.66.Bz

Understanding the interaction between optical radiation and individual subwavelength objects is of fundamental importance for the study of optical physics, and has practical significance for applications such as imaging, cloaking, biomedicine, and optical antennas [1–10]. The strength of this interaction is characterized by the scattering and the absorption cross sections, defined as $C_{\mathrm{sct}} \equiv P_{\mathrm{sct}}/I_0$, $C_{\mathrm{abs}} \equiv P_{\mathrm{abs}}/I_0$. Here, I_0 is the intensity of an incident plane wave, P_{sct} and P_{abs} are the amount of power scattered or absorbed by the particle, respectively. When the subwavelength object is a single atom in a three-dimensional (3D) vacuum, one can rigorously prove that its maximum scattering cross section is $(2l+1)\lambda^2/2\pi$ at the atomic resonant frequency, where l is the total angular momentum of the atomic transition involved. This limit becomes $3\lambda^2/2\pi$ for a typical electric dipole transition [11]. Theoretically, in two dimensions, one can similarly prove that the maximum cross section of an atom cannot exceed $2\lambda/\pi$. These limits in 3D or 2D, for reasons apparent from standard scattering theory that we will reiterate in this Letter, will be referred to as the single-channel limit. For subwavelength nanoparticles and nanowires, a common observation has been that the cross section is typically less than such single-channel limit [2,4,6,8–10]. But there have in fact been a few reports where the cross section goes somewhat beyond such a limit [12].

In this Letter, we provide a theoretical discussion on the limit of the scattering and absorption cross sections of a subwavelength structure. The theory indicates that, on the one hand, most of the nanostructures indeed should have their maximum cross section subject to the single-channel limit, and on the other hand, in plasmonic nanoparticles or nanowires, there is in fact a substantial opportunity to significantly overcome this limit. As a numerical demonstration, we present a subwavelength plasmonic structure where the scattering cross section is far beyond the single-channel limit, even in the presence of loss.

We start by briefly summarizing the relevant aspects in scattering theory. For simplicity, we will illustrate the main physics by considering the two-dimensional case where the obstacle is uniform in the z direction. Consider an obstacle located at the origin, surrounded by air. When a TM plane wave, defined by a wave vector $\mathbf{k}$, and with its magnetic field polarized along the z direction, impinges on the obstacle, the total field in the air region outside the scatterer is

$$H_{\mathrm{total}} = H_0\left(e^{i\mathbf{k}\cdot\mathbf{r}} + \sum_{m=-\infty}^{\infty} i^m S_m H_m^{(1)}(k\rho)e^{im\theta}\right). \quad (1)$$

Here, we use the convention that the field varies in time as $\exp(-i\omega t)$. (ρ, θ) are the polar coordinates centered at the origin. $H_m^{(1)}$ is the mth order Hankel function of the first kind, and represents an outgoing wave in the far field. The mth term in the summation thus defines the scattered wave in the mth angular momentum channel. S_m is referred to as the scattering coefficient. With the choice of $H_0 = 1\sqrt{\frac{\mathrm{Watt}}{\mathrm{meter}}\frac{\omega\varepsilon_0}{2}}$, $|S_m|^2$ represents the scattered power, normalized by the unit of power which is $\frac{\mathrm{Watt}}{\mathrm{meter}}$ in 2D.

The scattering coefficient S_m is in fact strongly constrained by energy conservation consideration. To see this, we express Eq. (1) alternatively as a summation of incoming and outgoing waves in each channel:

$$H_{\mathrm{total}} = \sum_{m=-\infty}^{\infty} H_0[h_m^+ H_m^{(2)}(k\rho) + h_m^- H_m^{(1)}(k\rho)]e^{im\theta} \quad (2)$$

where $H_m^{(2)}$ is the mth order Hankel function of the second kind that represents the incoming wave. $h_m^+ = i^m/2$ and $h_m^- = i^m(S_m + 1/2)$ are the incoming and outgoing wave amplitudes, respectively. With our choice of H_0, $|h_m^+|^2$ and $|h_m^-|^2$ represent the power carried by incoming and outgoing waves in the mth channel. Moreover, for systems with cylindrical symmetry, the angular momentum is conserved. Consequently, by energy conservation, the reflection coefficient defined as

$$R_m \equiv \frac{h_m^-}{h_m^+} = 1 + 2S_m \quad (3)$$

is subject to

$$|R_m| \leq 1. \quad (4)$$

For such a scatterer, the total scattered power is $P_{\text{sct}} = \sum_m |S_m|^2$, while the total absorbed power is $P_{\text{abs}} = \sum_m \frac{1}{4}(1 - |R_m|^2)$. On the other hand, the incident wave has an intensity $I_0 = \frac{\pi}{2\lambda}\frac{\text{Watt}}{\text{meter}}$. As a result, the total scattering and absorption cross sections become:

$$C_{\text{sct}} = \sum_{m=-\infty}^{\infty} \frac{2\lambda}{\pi}\left|\frac{R_m - 1}{2}\right|^2 \equiv \sum_{m=-\infty}^{\infty} C_{\text{sct},m}$$
$$C_{\text{abs}} = \sum_{m=-\infty}^{\infty} \frac{\lambda}{2\pi}(1 - |R_m|^2) \equiv \sum_{m=-\infty}^{\infty} C_{\text{abs},m}. \quad (5)$$

Using Eq. (4), one can immediately infer that the maximal contribution of a single channel to the scattering and absorption cross section is $\frac{2\lambda}{\pi}$ and $\frac{\lambda}{2\pi}$, respectively. The strongest scattering occurs when $R_m = -1$, while the strongest absorption occurs when $R_m = 0$.

For subwavelength particles, one can maximize the scattering cross section of a single channel by introducing a resonance. In the presence of a resonance in the mth channel, the scattering process can be modeled by the temporal coupled-mode equations [13,14]:

$$\frac{dc}{dt} = (-i\omega_0 - \gamma_0 - \gamma)c + i\sqrt{2\gamma}h^+$$
$$h^- = h^+ + i\sqrt{2\gamma}c, \quad (6)$$

where c is an amplitude and normalized such that $|c|^2$ corresponds to the energy of the resonance, ω_0 is the resonant frequency, γ_0 is the intrinsic loss rate due to material absorption, and γ is the external leakage rate due to the coupling of the resonance to the outgoing wave. All variables in Eq. (6) are specific to the mth channel. For notation simplicity we suppress the subscript m in Eq. (6). In deriving Eq. (6), we assume that, away from the resonant frequency, the scattering from the particle is negligible, hence $h^- \approx h^+$ when $c \approx 0$ [14]. For an incident wave at a frequency ω, the reflection coefficient can be obtained from Eq. (6):

$$R_m = \frac{i(\omega_0 - \omega) + \gamma_0 - \gamma}{i(\omega_0 - \omega) + \gamma_0 + \gamma}. \quad (7)$$

Substituting Eq. (7) to (5), we have

$$C_{\text{sct},m} = \frac{2\lambda}{\pi}\frac{\gamma^2}{(\omega - \omega_0)^2 + (\gamma_0 + \gamma)^2} \quad (8a)$$
$$C_{\text{abs},m} = \frac{2\lambda}{\pi}\frac{\gamma\gamma_0}{(\omega - \omega_0)^2 + (\gamma_0 + \gamma)^2}. \quad (8b)$$

The scattering cross section thus exhibits a Lorentzian spectral line shape, reaching a maximum of $\frac{2\lambda}{\pi}\frac{\gamma^2}{(\gamma_0+\gamma)^2}$ at the resonant frequency ω_0. In the strong overcoupling limit, i.e. $\gamma \gg \gamma_0$, at the resonant frequency the scattering cross section of a single channel can approach the maximal value of $\frac{2\lambda}{\pi}$.

The analysis above, especially Eq. (5), reproduces the results of standard scattering theory [15]. We repeat these analysis here, however, to emphasize that while there is a rigorous upper limit on cross sections in each individual scattering channel, there is no general theoretical constraint on the total cross section for an object with a given geometric dimension. Rather, in principle, arbitrarily large total cross sections can be reached, provided that one maximizes contributions from a sufficiently large number of channels.

For subwavelength objects, those angular momentum channels that do not support a resonance typically have very small contributions to the total scattering cross section. Therefore, if resonance is present in only one angular momentum channel, the *total* scattering cross section becomes constrained by the single-channel limit ($2\lambda/\pi$ in 2D, and $(2l + 1)\lambda^2/2\pi$ in 3D), as observed by a large number of studies [2,4,6,8–10]. In contrast, we will show that one can in fact significantly overcome such a single-channel limit, by creating resonances in large numbers of channels, by ensuring that these resonances all operate in the strong overcoupling limit, and by aligning their resonant frequencies. Below, we will refer to a subwavelength object having a scattering cross section that far exceeds the single-channel limit as a superscatterer.

To design a superscatterer we consider the nanorod schematically shown in the inset of Fig. 1, which consists of multiple concentric layers of dielectric and plasmonic materials. The plasmonic material is described by the Drude model with $\varepsilon = 1 - \omega_p^2/(\omega^2 + i\gamma_d\omega)$. The dielectric material has $\varepsilon = 12.96$. Similar structures have been experimentally explored before for other purposes [7,9].

We consider a lossless structure first by setting $\gamma_d = 0$. The property of the cylindrical structure as shown in Fig. 1

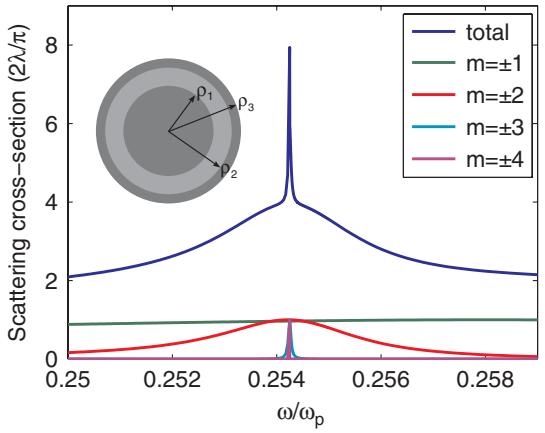

FIG. 1 (color online). Total scattering cross section of a nanorod in the lossless case, and the contributions from individual channels. The $m = \pm 1$ channel is near resonant in the plotted frequency range. Its resonant line shape is not apparent since its resonant linewidth is much larger than the frequency range plotted here. (Inset) Schematic of the nanorod. The dark gray and light gray areas correspond to a plasmonic material and a dielectric material, respectively. The geometry parameters are $\rho_1 = 0.3485\lambda_p$, $\rho_2 = 0.5623\lambda_p$, and $\rho_3 = 0.6370\lambda_p$, where $\lambda_p = 2\pi c/\omega_p$, with c being the speed of light in vacuum.

can be understood by first analyzing a corresponding planar structure (Inset of Fig. 2). For the TM wave, the corresponding planar structure supports three photonic bands (solid lines in Fig. 2). Two of them are associated with the dielectric layer. When sandwiched between two semi-infinite metal regions, a thin dielectric layer supports the lower and upper bands (dashed lines in Fig. 2) [16]. With a proper choice of the dielectric layer thickness, the upper band can be made flat [17]. In the planar structure considered here, since one of the metal regions has a finite thickness, this upper band anticrosses with the surface plasmon band at the metal-air interface (dotted line in Fig. 2), resulting in the band structure shown as solid lines in Fig. 2.

Starting from modes in the corresponding planar structure, the resonances of the nanorod can be understood using the whispering gallery condition [14,18]. The nanorod supports the mth order resonance at a frequency ω, when the propagation constant β of a mode in the corresponding planar structure satisfies:

$$\beta 2\pi r_0 = 2\pi m, \tag{9}$$

where $r_0 = (\rho_1 + \rho_2)/2$. Thus, the existence of a flat band in the planar structure should directly translate into near degeneracy in terms of frequencies between nanorod resonances at different angular momentum channels.

We plot the resonant frequencies and the leakage rates of the nanorod as a function of $|m|/r_0$ in Fig. 2. We indeed observe resonances between $m = -4$ and $m = +4$, all lying close to the frequency of $0.2542\omega_p$ where the planar structure has a flat band. The positions of these resonances in general agree quite well with Eq. (9), with a better agreement observed for larger angular momentum channels [18]. Also, the leakage rates of these resonances decease as one increases the angular momentum, in consistency with Refs. [8,15,19].

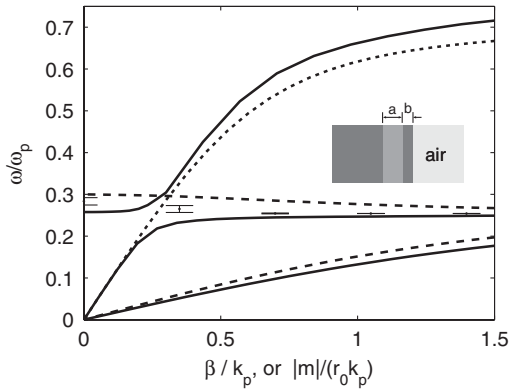

FIG. 2. A planar structure. The dark and light gray regions correspond to metal and dielectric material, respectively. $a = \rho_2 - \rho_1$, $b = \rho_3 - \rho_2$. (Main Figure) The solid lines are the dispersion curves for the structure shown in the inset. The dashed and dotted lines represent the dispersion curves for a corresponding metal-dielectric-metal structure, and the metal-air interface, respectively. The bars represent the properties of the resonance in the scatterer at different angular momentum channels labeled by m. The center and the height of each bar correspond to the resonant frequency and the leakage rate, respectively.

The spectra for the scattering cross section of the nanorod are shown in Fig. 1. The total scattering cross section reaches a peak value of $7.94(2\lambda/\pi)$, which is far beyond the single-channel limit, even though the scatterer just has a subwavelength diameter of 0.32λ. Such a large total scattering cross section is a result of the near degeneracy of resonances in multiple channels. The contribution from each channel between $m = \pm 1$ and $m = \pm 4$ has a Lorentzian line shape that peaks with a value of $2\lambda/\pi$, at a frequency around $0.2542\omega_p$ (Fig. 1).

Figure 3(a) plots the real part of the total field distribution and the Poynting vector lines at the frequency of $0.2542\omega_p$, when a plane wave, with unity amplitude, illuminates the nanorod. The nanorod leaves a large ''shadow'' behind it. The size of the shadow is much larger than the diameter of the rod. The presence of the rod also leads to significant redistribution of the power flow around the rod [Fig. 3(a)].

We emphasize that the superscattering effect is not an automatic outcome with the use of plasmonic material. A uniform plasmonic cylinder of the same size has a much smaller scattering cross section [Fig. 3(b)].

We now consider the lossy case. For the damping constant in the Drude model, we use $\gamma_d = \gamma_{\text{bulk}} + A \times V_F/l_r$ in order to take into account both the bulk and the surface scattering effects [20]. Here $\gamma_{\text{bulk}} = 0.002\omega_p$ is appropriate for the bulk silver at the room temperature [21], $A \approx 1$ [20], $V_F = 7.37 \times 10^{-4}\lambda_p\omega_p$ is the Fermi velocity for silver [22], and l_r is the electron mean free path. In our structure, for the metallic core, we take $l_r = \rho_1$ and hence $\gamma_d = 0.004\omega_p$; for the metallic shell, we take $l_r = \rho_3 - \rho_2$ and hence $\gamma_d = 0.012\omega_p$. The total scattering cross section at the peak frequency of $0.2542\omega_p$ is $1.92(2\lambda/\pi)$ [Fig. 4(a)], which is still about 2 times the single-channel limit. The contributions to scattering are mostly from the $m = \pm 1, \pm 2$ channels. In the higher angular momentum channels, the loss rate dominates over the radiation leakage rate. These resonances are therefore no longer in the over-

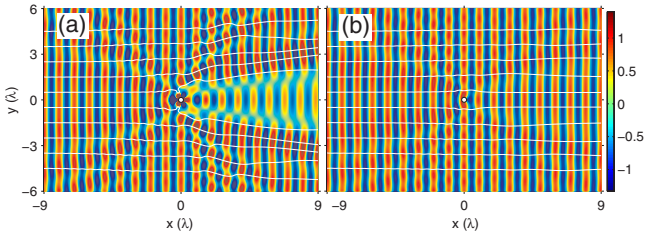

FIG. 3 (color online). Real part of the total field distribution and the Poynting vector lines at the frequency of $0.2542\omega_p$ (a) for the nanorod shown in Fig. 1, (b) when the rod is replaced by a same-size uniform plasmonic cylinder. Here the amplitude of an incident plane wave is unity. The white circle at the center indicates the size of the rod.

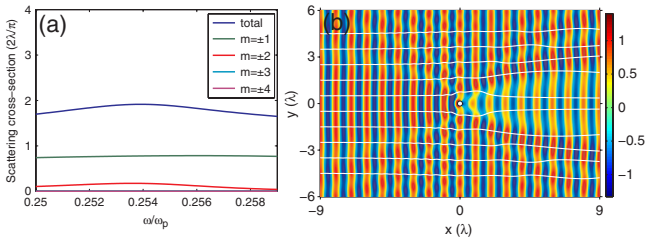

FIG. 4 (color online). (a) Total scattering cross section of the nanorod for the lossy case of realistic silver, and the contributions from each individual channel. The $m = \pm 1$ channel is near resonant in the plotted frequency range. Its resonant line shape is not apparent since its resonant linewidth is much larger than the frequency range plotted here. (b) Field distributions and the Poynting vector lines at the frequency $0.2542\omega_p$.

coupled limit and do not contribute significantly to the scattering. Since the radiation leakage rate is generally smaller for the higher angular momentum channel [8,15,19], the presence of loss has a more significant effect in the higher angular momentum channels in general. Nevertheless, our results show that a superscatterer can be designed even in the presence of realistic loss. Figure 4(b) plots the total field distribution and the Poynting vector lines at the frequency of $0.2542\omega_p$ for the lossy case. All the visual signature of the superscattering effect is still quite evident.

For the same structure, the absorption cross section has a peak of $0.73(2\lambda/\pi)$ at the frequency of $0.2542\omega_p$. Thus this structure has a scattering cross section that significantly dominates over its absorption cross section. In general, for a given channel, the absorption cross section is maximized at the critical coupling when $\gamma = \gamma_0$ [cf. Eq. (8b)]. Based our theory, therefore, we can seek to either maximize or minimize the total absorption cross section as well.

We remark that in the literature, sometimes the scattering efficiency, which is defined as the ratio of the scattering cross section over the geometrical cross section, rather than the scattering cross section itself, is optimized. An example of a subwavelength object that has a very large scattering efficiency is in fact an atom, since an atom has a scattering cross section that is at the wavelength scale on resonance [11], and a very small geometrical cross section. One may regard subwavelength particles as electromagnetic ''meta-atoms''. From this consideration, it is very unlikely that such a ''meta-atom'' can outperform a real atom in terms of scattering efficiency. Instead, our results here indicate that such a ''meta-atom'' can have an electromagnetic cross section beyond what an atom can achieve, and thus represents a fundamentally new capability.

We end by contrasting our superscatterer with some of the related works. In Refs. [23,24], the concept of transformation optics has been used to drastically enhance the scattering cross section of a particle. To implement these concepts, however, it requires a material whose both permittivity and permeability are highly inhomogeneous and anisotropic. In contrast, our design requires only conventional plasmonic and dielectric materials. Also, it is well known that the cross section of an antenna can be drastically enhanced by making the antenna directional [25]. Our approach is fundamentally different—our designed structure is isotropic due to the cylindrical symmetry. Finally, we have in fact generalized the idea to three dimensions and designed subwavelength spherical particles with scattering cross section significantly higher than the single-channel limit of $(2l + 1)\lambda^2/2\pi$ [26].

The authors acknowledge the support of the Interconnect Focus Center, funded under the Focus Center Research Program (FCRP), a Semiconductor Research Corporation entity, and the DOE Grant No. DE-FG 07ER46426.

[1] S. Nie *et al.*, Science **275**, 1102 (1997).
[2] J. B. Jackson *et al.*, Proc. Natl. Acad. Sci. U.S.A. **101**, 17 930 (2004).
[3] L. R. Hirsch *et al.*, Proc. Natl. Acad. Sci. U.S.A. **100**, 13 549 (2003); A. Barhoumi *et al.*, Chem. Phys. Lett. **482**, 171 (2009).
[4] J. Aizpurua *et al.*, Phys. Rev. Lett. **90**, 057401 (2003).
[5] A. Alù and N. Engheta, Phys. Rev. Lett. **100**, 113901 (2008).
[6] J. A. Schuller *et al.*, Nat. Photon. **3**, 658 (2009).
[7] F. Hao *et al.*, Nano Lett. **8**, 3983 (2008).
[8] M. I. Tribelsky and B. S. Lykyanchuk, Phys. Rev. Lett. **97**, 263902 (2006).
[9] R. Bardhan *et al.*, J. Phys. Chem. C **114**, 7378 (2010).
[10] A. E. Miroshnichenko, Phys. Rev. A **80**, 013808 (2009).
[11] C. J. Foot, *Atomic Physics* (Oxford University Press, New York, 2005), pp. 140–142.
[12] K. L. Kelly *et al.*, J. Phys. Chem. B **107**, 668 (2003); P. K. Jain *et al.*, *ibid.* **110**, 7238 (2006).
[13] R. E. Hamam *et al.*, Phys. Rev. A **75**, 053801 (2007).
[14] Z. Ruan *et al.*, J. Phys. Chem. C **114**, 7324 (2010).
[15] H. C. van de Hulst, *Light Scattering by Small Particles* (Dover, New York, 1981).
[16] E. N. Economou, Phys. Rev. **182**, 539 (1969); H. Shin and S. Fan, Phys. Rev. Lett. **96**, 073907 (2006).
[17] H. Shin *et al.*, Appl. Phys. Lett. **89**, 151102 (2006).
[18] P. B. Catrysse *et al.*, Appl. Phys. Lett. **94**, 231111 (2009).
[19] Z. Jacob *et al.*, Opt. Express **14**, 8247 (2006).
[20] R. D. Averitt, D. Sarkar, and N. J. HalasPhys. Rev. Lett. **78**, 4217 (1997).
[21] M. Ordal *et al.*, Appl. Opt. **22**, 1099 (1983).
[22] C. Kittel and P. McEuen, *Introduction to Solid State Physics* (Wiley, New York, 1996).
[23] T. Yang *et al.*, Opt. Express **16**, 18 545 (2008).
[24] W. Wee *et al.*, New J. Phys. **11**, 073033 (2009).
[25] C. A. Balanis, *Antenna Theory: Analysis and Design* (Wiley, New York, 1996), 2nd ed.
[26] Z. Ruan and S. Fan, (unpublished).